Published in final edited form as:
Cancer Res. 2009 March 15; 69(6): 2599. doi:10.1158/0008-5472.CAN-08-2595.

U19/Eaf2 Binds to and Stabilizes von Hippel-Lindau Protein

Wuhan Xiao[1,6], **Junkui Ai**[1], **Geoffrey Habermacher**[3], **Olga Volpert**[3], **Ximing Yang**[4], **Ai-yuan Zhang**[1], **Junghyun Hahn**[3], **Xiaoyan Cai**[3], and **Zhou Wang**[1,2,3,5]

[1] Department of Urology, University of Pittsburgh, Pittsburgh, Pennsylvania

[2] University of Pittsburgh Cancer Institute, University of Pittsburgh, Pittsburgh, Pennsylvania

[3] Department of Urology, Northwestern University, Chicago, Illinois

[4] Department of Pathology, Northwestern University, Chicago, Illinois

[5] Robert H. Lurie Comprehensive Cancer Center, Feinberg School of Medicine, Northwestern University, Chicago, Illinois

[6] Institute of Hydrobiology, Chinese Academy of Sciences, Wuhan, People's Republic of China

Abstract

Studies have firmly established a key regulatory role for the tumor suppressor pVHL in the regulation of the vascular system and normal spermatogenesis. Here, we report that knockout of the newly identified tumor suppressor U19/Eaf2 also caused vascular system abnormalities and aspermatogenesis, suggesting a potential link between U19/Eaf2 and pVHL. Coimmunoprecipitation and *in vitro* binding assays showed an association between U19/Eaf2 and pVHL, whereas deletion mutagenesis revealed the requirement of the NH_2 terminus of U19/Eaf2 and both the α and β domains of pVHL for this binding. U19/Eaf2 stabilizes pVHL, as shown by protein stability and pulse-chase studies. Testes and mouse embryonic fibroblasts (MEF) derived from *U19/Eaf2* knockout mice expressed reduced levels of pVHL, indicating that full *in vivo* expression of pVHL indeed requires U19/Eaf2. As expected, *U19/Eaf2* knockout MEF cells exhibited an increased level and activity of hypoxia-inducible factor 1α (HIF1α), a protein typically regulated via a pVHL-mediated degradation pathway. Furthermore, angiogenesis in a Matrigel plug assay was significantly increased in *U19/Eaf2* knockout mice. The above observations argue that U19/Eaf2 can modulate HIF1α and angiogenesis, possibly via direct binding and stabilization of pVHL.

Introduction

Carriers of germ-line mutations in the *von Hippel-Lindau* (*VHL*) gene are predisposed to the VHL syndrome. This autosomal dominant syndrome has multiple manifestations, including high incidence of clear cell renal carcinoma, hemangioblastomas, and pheochromocytomas (1–4). Conventional *VHL* deletion in the mouse is embryonic lethal due to vascular abnormalities in the placenta (5). However, mice with conditional *VHL* deletions survive, and studies using these mice further support a tumor-suppressive role for pVHL (6,7). Targeted deletion of *VHL* in the livers of BALB/c mice resulted in the hypervascularization of the liver parenchyma (6). Mice with tissue-specific *VHL* deletions also developed hepatic vascular

Requests for reprints: Zhou Wang, University of Pittsburgh Medical College, Suite G40, 5200 Centre Avenue, Pittsburgh, PA 15232. Phone: 412-623-3903; Fax: 412-623-3904; wangz2@upmc.edu.
Note: W. Xiao and J. Ai are co-first authors.

Disclosure of Potential Conflicts of Interest
No potential conflicts of interest were disclosed.

tumors, angiectasis in multiple organs, and defects in spermatogenesis (7), pointing to the essential role of pVHL in the homeostasis of multiple tissues.

pVHL contributes to the regulation of oxygen-responsive gene expression by targeting the transcription factor hypoxia-inducible factor 1α (HIF1α) for proteasomal degradation under normoxic conditions (8,9). In a mechanism analogous to the SCF (Skp1/Cdc53/F-box) ubiquitination machinery, pVHL targets HIF1α for degradation by serving as a bridge between HIF1α and a multiprotein E3 ubiquitin ligase complex consisting of elongin C, elongin B, Cul-2, and Rbx 1 (10–13). In this capacity, pVHL acts in a manner similar to an F-box protein (9). pVHL has two main domains: α domain (residues 155–192) and β domain (residues 63–154 and 193–204; ref. 14). The α domain binds to the E3 ubiquitin ligase complex via elongin C (15,16), whereas the β domain contains the substrate recognition motif for HIF1α. Association of pVHL with HIF1α requires the hydroxylation of key proline residues (P402 and P564) within the oxygen degradation domain of HIF1α. Under normoxic or atmospheric O_2 levels (21%), a conserved family of prolyl-4-hydroxylases mediates hydroxylation of HIF1α, allowing pVHL to bind to and thus target HIF1α for ubiquitin-mediated proteasomal degradation (17–22). In contrast, limited O_2 inhibits proline hydroxylation, preventing the association between pVHL and HIF1α. Consequently, HIF1α accumulates and enters the nucleus, where it dimerizes with the constitutively stable HIF1β subunit to form the heterodimeric transcription factor HIF (20). As an active transcription factor, HIF acts as the primary regulator of both cellular and systemic responses to decreased O_2 concentration; responses include enhanced glycolysis, cell proliferation, apoptosis, erythropoiesis, and angiogenesis (23). Loss of pVHL, therefore, leads to the constitutive activation of HIF1α and its target genes, mimicking a state of constant hypoxia despite normal O_2 content. The inappropriately expressed HIF1α targets include vascular endothelial growth factor (VEGF), platelet-derived growth factor B, and mitogenic factors such as transforming growth factor α (24–26). Overproduction of the proangiogenic factors may explain the hypervascular nature of hemangioblastomas and renal cell carcinomas. Although HIF is a critical target of pVHL in the progression of hemangioblastomas and renal cell carcinoma, pVHL may also interact with other proteins critical to tumor suppression (27–29). Thus, the identification and characterization of additional pVHL binding partners will help elucidate the mechanism of pVHL-mediated tumor suppression and/or the regulation of pVHL function.

U19/Eaf2 is a newly identified tumor suppressor. We previously reported evidence for U19/Eaf2 down-regulation, allelic loss, promoter hypermethylation, and homozygous deletion in human advanced prostate cancer specimens. U19/Eaf2 is also implicated in acute myeloid leukemia. Consistent with its potential suppressive role in the human, *U19/Eaf2* knockout mice developed lung adenocarcinoma, hepatocellular carcinoma, B-cell lymphoma, and high-grade prostatic intraepithelial neoplasia (30). Here, we report that the *U19/Eaf2* knockout mice displayed abnormalities in vasculogenesis and spermatogenesis. *VHL* conditional knockout mice also developed abnormalities in vasculogenesis and spermatogenesis, suggesting a potential relationship between U19/Eaf2 and pVHL. Indeed, we present evidence that U19/Eaf2 can bind to and stabilize pVHL, thus blocking HIF-driven angiogenesis. Our data argue that U19/Eaf2 can modulate the pVHL pathway via direct binding and stabilization of pVHL.

Materials and Methods

Histologic analysis

Analyses were done using virgin male mice of ages 1 to 24 mo. Experimental cohorts were wild-type, heterozygous, and homozygous littermates with C57BL/6 and 129 combined genetic backgrounds. Tissue were fixed in 10% phosphate-buffered formalin at 4°C. Samples were then embedded in paraffin, sectioned at 5 μm, and stained with H&E. Immunohistochemical staining was done as described previously (30).

Cell culture and transfection

RCC4, 293, and Cos-7 cells were cultured in DMEM with 10% fetal bovine serum (FBS) and penicillin/streptomycin. RCC4/vec and RCC4/VHL (provided by Peter J. Ratcliffe, University of Oxford, Oxford, United Kingdom and Paul G. Corn, M. D. Anderson Cancer Center, Houston, TX) were cultured in DMEM with 10% FBS, 1 mg/mL G418, and penicillin/streptomycin. Primary mouse embryonic fibroblasts (MEF) were generated from embryonic day 12.5 (E12.5) to day 13.5 (E13.5) embryos from a mixed C57BL/6J/129 background. MEFs were immortalized by SV40T antigen (provided by Katherine Rundell, Northwestern University, Chicago, IL) and maintained in DMEM with 10% FBS, 0.1 mmol/L nonessential amino acids (Invitrogen), 100 μmol/L 2-mercaptoethanol (Sigma), and penicillin/streptomycin. Cos-7 and MEFs were transfected using Lipofectamine 2000 (Invitrogen). 293 cells were transfected using Fugene 6 (Roche).

Antibodies and chemical reagents

Anti-Flag (M2; monoclonal) and anti-c-Myc–conjugated agarose were purchased from Sigma. Monoclonal anti-hemagglutinin (HA) antibody was purchased from Covance Research Products. Anti–c-Myc (polyclonal), antimouse VHL (polyclonal), and anti-HA–conjugated agarose were purchased from Santa Cruz Biotechnology; antihuman VHL (monoclonal) and antihuman HIF1α (monoclonal) were purchased from BD Biosciences. Anti-HIF1α (NB-100-449) for mouse HIF1α detection was purchased from Novus Biologicals. Cycloheximide was purchased from Sigma.

Plasmids

We subcloned Myc-tagged pVHL, U19/Eaf2, and their mutants into pCMV-Myc vector (Clontech) at *Sal*I and *Kpn*I sites by PCR. Wild-type pcDNA VHL was a gift from Peter J. Ratcliffe. Flag-tagged VHL was a gift from Frank Lee (Belfast City Hospital, Belfast, United Kingdom). The hypoxia response element (HRE) and mutated HRE-luciferase reporter constructs were provided by Navdeep Chandel (Northwestern University, Chicago, IL). To obtain the construct for pVHL *in vitro* translation, we subcloned pVHL into pBluescript II KS + vector (Stratagene). Full-length pVHL and U19/Eaf2 cDNA were subcloned into pCG N3HAM vector (31) to generate HA-tagged proteins (a methionine-rich variant provided by William Tansey, Cold Spring Harbor Laboratory, New York, NY).

Immunoprecipitation and Western blotting

Wild-type Flag-pVHL and Myc-U19/Eaf2 or Myc empty vector were transiently transfected into Cos-7 cells. Wild-type Myc-U19/Eaf2 and HA-pVHL or HA empty vector were transiently transfected into 293 cells. After 28 h, cells were directly lysed in radioimmunoprecipitation assay (RIPA) buffer with complete protease inhibitors (Roche). For coimmunoprecipitation, we incubated 500 μg of whole-cell extract with 20 μL of Myc-agarose conjugate (Sigma) or 10μL of HA-agarose conjugate (Santa Cruz Biotechnology) for 16 h at 4°C. The immune complex was washed three to five times in RIPA buffer, separated by SDS-PAGE (NuPAGE 4–12% Bis-Tris Gel, Invitrogen), and analyzed by Western blot.

pVHL-expressing stable revertants of RCC4 (RCC4/VHL) were maintained in hypoxia (1% O_2) for 16 h to enhance U19/Eaf2 protein levels and lysed in RIPA buffer. For immunoprecipitation, we precleared 500 μg of whole-cell extract for 1 h with 20 μL of protein A/G-agarose beads (Santa Cruz Biotechnology) and 1 μg of normal mouse immunoglobulin, which were then incubated with 50 μL of a rabbit polyclonal antibody against human U19/Eaf2 or 1 μg of normal rabbit IgG for 16 h at 4°C. The immune complexes were washed in RIPA buffer, separated by SDS-PAGE, and analyzed by Western blot.

In vitro association experiment

Glutathione *S*-transferase (GST) and GST-U19/Eaf2 were purified from bacterial lysates using glutathione-agarose (Sigma). ^{35}S-labeled pVHL was translated *in vitro* using a TNT-coupled reticulocyte lysate system (Promega). After preincubation in 0.1% bovine serum albumin/PBS for 1 h, GST or GST-U19/Eaf2 bound to glutathione-agarose and ^{35}S-labeled pVHL were incubated at 4°C for 4 h. The beads were extensively washed five times with PBS containing 0.5% NP40 and 150 mmol/L NaCl before being subjected to SDS-PAGE followed by autoradiography.

Protein stabilization and pulse-chase experiment

We transiently transfected Cos-7 and 293 cells with 2 μg of Flag-VHL or HA-VHL with increasing amounts of Myc-U19 or Myc-U19 (114–260) complemented by up to 2 μg total of Myc empty vector. After 28 h, the transfected cells were directly lysed in RIPA buffer, separated by SDS-PAGE, and analyzed by Western blotting.

We transiently transfected 293 cells with HA-VHL and either Myc-U19 or Myc-U19 (114–260). After 24 h, cells were treated with cycloheximide at 50 μg/mL for 0, 2, 4, and 8 h (32). Then, the cells were directly lysed in RIPA buffer, separated by SDS-PAGE, and analyzed by Western blot.

For pulse-chase assays, HA-VHL and Myc-U19 or Myc empty vector were transiently transfected into 293 cells. After 48 h, cells were maintained in DMEM/10% FBS lacking Met and Cys for 1 h. Cells were then incubated in DMEM/10% FBS containing a [^{35}S]Met/Cys mixture (50 μCi/mL; Perkin-Elmer) for 2 h. The cells were then washed twice with warm PBS and labeling was stopped by addition of growth medium with Met and Cys (3 mmol/L).

Hypoxia treatment and luciferase assay

U19$^{+/+}$ and U19$^{-/-}$ MEFs were maintained in a hypoxia chamber (~1% O_2) for 16 h to achieve HIF1α stabilization and then released into normoxia. Lysates were collected at multiple time points for immunodetection of HIF1α. Cycloheximide was used to prevent any new synthesis of HIF1α during normoxia.

We transiently transfected HRE and mutated HRE-luciferase reporter constructs along with the *Renilla* luciferase reporter into MEFs of U19$^{+/+}$ and U19$^{-/-}$. After 6 h, the cells were placed in hypoxic conditions or maintained in normoxia for 20 h and then directly lysed using PLB buffer supplied by Dual Luciferase Reporter Assay system (Promega). The luciferase activity was determined using a luminometer (Sirius, Zylux Corp.) and normalized to *Renilla* luciferase activity. Data are reported as mean ± SE of two separate experiments done in triplicate.

Matrigel plug angiogenesis assay

Age-matched *U19/Eaf2* wild-type and *U19/Eaf2*-null mice (~6 mo old) were injected with 0.5 mL Matrigel (BD Biosciences) containing 2 ng/mL VEGF and 69 units/mL heparin. Three female and three male mice were used for each group. After 12 d, Matrigel plugs were removed for frozen sectioning. Matrigel sections (5 μm) were incubated with rat anti-mouse CD31 antibody (Pharmingen) followed by rhodamine-conjugated donkey anti-rat antibody (Jackson ImmunoResearch). Digital images were obtained with a Nikon TE2000-U fluorescent microscope and quantified for microvascular density with ImageJ software.

Results

U19/Eaf2 gene deletion causes late-onset aspermatogenesis and extramedullary hematopoiesis

In our recently generated *U19/Eaf2* knockout mice, we had observed cardiac enlargement, lung adenocarcinoma, hepatocellular carcinoma, B-cell lymphoma, and high-grade prostatic intraepithelial neoplasia (30). The mice also developed noncancerous phenotypes, such as aspermatogenesis seen in older animals (Fig. 1*A*–*C*). Human, mouse, and rat testes all express U19/Eaf2 (data not shown), suggesting a possible role in testicular function. Within 2 to 3 months of age, no reproduction abnormalities were detected in *U19/Eaf2*-null males or females (data not shown). However, at 22 months or older, 26.1% (12 of 46) of *U19/Eaf2*-null male mice exhibited a dramatic reduction in their testis size and wet weight; testes from null animals weighed ~60% less ($P < 0.05$; Fig. 1*A* and *C*). H&E staining revealed that these abnormal testes contained degenerated germ cells filled with vacuoles; multinucleated giant cells, reflecting abnormal sperm maturation; and few Sertoli cells (Fig. 1*A*). Cross sections of the *U19/Eaf2* knockout testes showed seminiferous tubule atrophy and collapse of the testicular capsule, with few sperm in the seminiferous tubule. Terminal deoxyribonucleotidyl transferase–mediated dUTP nick end labeling (TUNEL) staining revealed large numbers of germ cells undergoing apoptosis in *U19/Eaf2*-null males (Fig. 1*A*). These data indicate an important role of U19/Eaf2 in normal spermatogenesis during adulthood. Moreover, no testicular abnormality was observed in a cohort of 15 U19/Eaf2 heterozygotes and 20 wild-type mice (data not shown), suggesting that one copy of *U19/Eaf2* is sufficient for normal development and maintenance of the testis.

We observed that two of the *U19/Eaf2* knockout mice developed extramedullary hematopoiesis, accompanied by extreme enlargement of the spleen and liver (Fig. 1*D*). Histologic examination revealed spleen tissue filled with hematopoietic cells and immature blood cells at different stages, cells that normally exist in the bone marrow. More Ki-67–positive cells were present in the spleen of *U19/Eaf2*-null mice as compared with wild-type controls (Fig. 1*D*). Given the high expression level of U19/Eaf2 in bone marrow (33), *U19/Eaf2* inactivation may disrupt the normal hematopoiesis in bone marrow, causing a compensatory response from spleen and liver. We recognize the possibility that an unrelated sporadic mutation may cause this phenotype because only 2 of 46 *U19/Eaf2*-null mice developed extramedullary hematopoiesis. However, we have never observed this phenotype in all of the wild-type or *U19/Eaf2* heterozygotes in our lab, suggesting that the *U19/Eaf2* knockout is likely responsible.

U19/Eaf2 protein binds to pVHL directly

Our studies showed that *U19/Eaf2*-null mice displayed defects in spermatogenesis (Fig. 1*A*) and in the vascular system, including heart enlargement (30) and extramedullary hematopoiesis (Fig. 1*D*). Work from others had established that conditional knockout of *VHL*, a well-characterized tumor suppressor in renal cell carcinoma, also causes defects in spermatogenesis and vascular system (7). Together, these observations led us to speculate that a functional link may exist between U19/Eaf2 and the VHL pathway. We first analyzed the possibility of a physical interaction between U19/Eaf2 and pVHL proteins by transiently coexpressing Myc-tagged U19/Eaf2 with Flag-tagged pVHL in either monkey kidney Cos-7 cells or human kidney 293 cells. Immunoprecipitation followed by Western blot analysis showed that Flag-pVHL coprecipitated with Myc-U19/Eaf2, but not in vector-transfected controls (Fig. 2*A*). Similarly, Myc-U19/Eaf2 coprecipitated with HA-tagged pVHL (HA-pVHL; Fig. 2*B*), pointing to a specific association between exogenous U19/Eaf2 and pVHL. The reciprocal coimmunoprecipitation was done in both cell lines and was reproducible (data not shown), indicating that the cell lines used did not affect the association.

To test whether pVHL and endogenous U19/Eaf2 proteins interact, we performed coimmunoprecipitation experiments using RCC4 renal cancer cells expressing HA-tagged wild-type pVHL. We incubated cells under hypoxic conditions (1% O_2) for 16 hours before the cell extract preparation because we have found that this increases U19/Eaf2 protein levels (data not shown). Antibody to U19/Eaf2 coprecipitated HA-pVHL, whereas isotype control IgG did not (Fig. 2*C*), arguing for an *in vivo* association between U19/Eaf2 and pVHL.

To assess whether U19/Eaf2 binds to pVHL directly, we performed *in vitro* binding assays using bacterially expressed and purified GST-U19/Eaf2 and *in vitro* translated ^{35}S-labeled pVHL. Figure 2*D* shows that pVHL bound GST-U19/Eaf2, but not GST alone, indicating a direct association between wild-type U19/Eaf2 and pVHL.

To further characterize the interaction between U19/Eaf2 and pVHL, we carried out domain mapping for both U19/Eaf2 and pVHL. We constructed eight different deletion mutants of U19/Eaf2 and tested their ability to bind pVHL *in vivo* (Fig. 3*A*). This analysis revealed that pVHL bound to the NH_2 terminus of U19/Eaf2 (residues 1–113) but not to the COOH terminus (residues 114–260; Fig. 3*A*). We also constructed five deletion mutants of pVHL for use in coimmunoprecipitation experiments (Fig. 3*B*). pVHL required both its α and β domains to bind U19/Eaf2. Furthermore, the VHL mutant (residues 1–192) lacking the minor β domain (residues 193–204) displayed a decrease in U19/Eaf2 binding as compared with the VHL mutant (residues 1–206) containing the entire α and β domains. These data show that both the α and β domains are required for pVHL to bind U19/Eaf2.

U19/Eaf2 binding causes an increase in pVHL stability

While studying U19/Eaf2-pVHL interactions, we observed an increase in Flag-pVHL levels when it was cotransfected with Myc-U19/Eaf2 as compared with control vector (Fig. 2*A*). Similarly, Myc-U19/Eaf2 protein levels also increased with the cotransfection of Myc-U19/Eaf2 with HA-pVHL (Fig. 2*B*). These observations suggest that the association of U19/Eaf2 and pVHL might result in the stabilization of both proteins.

To examine the possibility of pVHL stabilization by U19/Eaf2, we transiently transfected 2 μg of the Flag-VHL expression vector with increasing amounts of Myc-U19/Eaf2, complemented by Myc empty vector to maintain equal DNA amount (total 2 μg) into Cos-7 cells. We then measured VHL protein levels by blotting for Flag. Cells transfected with increasing amounts of Myc-U19/Eaf2 showed a corresponding increase in the Flag-VHL protein (Fig. 4*A*). In contrast, HA-pVHL levels remained constant in the presence of the NH_2-terminal deletion U19/Eaf2 mutant (114–260), which does not bind to pVHL (Fig. 4*A*). These results indicate that U19 stabilizes pVHL and identify the NH_2-terminal region (1–113) of U19 as critical for this stabilization.

We further evaluated the effect of U19/Eaf2 on pVHL stability using the protein synthesis inhibitor cycloheximide and pulse-chase experiments. We transfected HA-pVHL expression vector with Myc-U19/Eaf2, empty vector, or Myc-U19/Eaf2 (114–260) into 293 cells and, 24 hours later, treated cells with cycloheximide. Using Western blot analysis, we showed that in the presence of wild-type U19/Eaf2, the estimated half-life of HA-pVHL was longer than 8 hours (Fig. 4*B*). In contrast, when cells were cotransfected with empty vector control or the deletion mutant Myc-U19/Eaf2 (114–260), the estimated half-life of pVHL was no greater than 2 and 4 hours, respectively (Fig. 4*B*). The pulse-chase analysis further confirmed the ability of U19/Eaf2 to prolong the half-life of pVHL (Fig. 4*C*). The above observations show that U19/Eaf2 enhances pVHL stability.

U19/Eaf2 knockout testes have reduced levels of pVHL

To determine if the endogenous pVHL level is decreased in the *U19/Eaf2* knockout mice, we performed Western blot analysis with an anti-pVHL antibody. Given that the aspermatogenesis phenotype was observed in both *VHL* conditional knockout and *U19/Eaf2*-null mice, we initially measured VHL protein levels in the testes of *U19/Eaf2* wild-type and *U19/Eaf2*-null mice. As expected, endogenous expression of pVHL was higher in the wild-type than in the *U19/Eaf2*-null testes (Fig. 4*D*). The endogenous pVHL protein levels in other major organs, including kidney, lung, and heart, were also reduced in the *U19/Eaf2*-null mice; however, the reduction was not as dramatic as that in testes (data not shown). Furthermore, endogenous pVHL levels in the U19/Eaf2-null MEF cells were lower than those in the wild-type MEF cells (Fig. 4*D*). To test whether U19/Eaf2 affects pVHL transcription, we carried out real-time reverse transcription-PCR analysis for VHL mRNA in 293 cells overexpressing U19/Eaf2 or control vector, testes from *U19/Eaf2*-null and wild-type mice, and $U19^{+/+}$ and $U19^{-/-}$ MEF cells. These experiments revealed no difference in the VHL transcript levels in the matched sample pairs (data not shown). These data indicate that U19/Eaf2 influences pVHL level posttranscriptionally by stabilizing pVHL protein through direct binding.

U19/Eaf2 deletion enhances HIF1α level and angiogenesis

A well-documented function of pVHL is the targeting of HIF for oxygen-dependent proteolysis (8,9). Given our finding that U19/Eaf2 binds to and stabilizes pVHL, we investigated whether U19/Eaf2 had any effect on the pVHL-mediated degradation of HIF1α in immortalized $U19^{+/+}$ and $U19^{-/-}$ MEFs. As expected, the endogenous HIF1α level was higher in $U19^{-/-}$ cells than in $U19^{+/+}$ cells, particularly under hypoxic conditions (Fig. 5*A*). When wild-type MEF cells were switched from hypoxia to normoxia, the majority of HIF1α was degraded within 5 minutes. In contrast, in U19/Eaf2-null MEF cells switched from hypoxia to normoxia, HIF1α was only partially degraded at 5 minutes or even 10 minutes after the switch. These results argue that U19/Eaf2 modulates the degradation of HIF1α, presumably mediated by pVHL.

We next examined the transcriptional activity of HIF1α in $U19^{+/+}$ and $U19^{-/-}$ MEF cells using a HRE-driven luciferase reporter (34). The HIF1α transcriptional activities in both *U19/Eaf2*-null and wild-type MEF cells were markedly induced under hypoxic conditions (Fig. 5*B*). As expected, the levels of HIF1α transcriptional activation in $U19^{-/-}$ MEF cells were higher than those in $U19^{+/+}$ cells, indicating a role of U19/Eaf2 in regulating HIF1α function. As a control, we showed that a mutant HRE construct with deleted HIF binding sites did not respond to the hypoxic induction of transcriptional activity in both $U19^{+/+}$ and $U19^{-/-}$ MEF cells.

Because U19/Eaf2 mediated efficient degradation of HIF1α, we next tested whether U19/Eaf2 could influence angiogenesis in the Matrigel plug assay (35,36). Immunostaining with anti-CD31 antibody followed by quantitative analysis showed that the microvessel density in Matrigel plugs containing 2 ng/mL VEGF was ~3.5-fold higher in the *U19/Eaf2*-null mice relative to the wild-type mice, and the difference was statistically significant ($P < 0.05$; Fig. 6). This finding argues that U19/Eaf2 plays a role in regulating angiogenesis in cooperation with pVHL via the HIF1α pathway.

Discussion

We recently identified U19/Eaf2 as a tumor suppressor in multiple mouse tissues and possibly also in humans (30,33). In this article, we show that *U19/Eaf2*-null mice develop noncancerous phenotypes that overlap with those observed in VHL conditional knockout mice. Furthermore,

we present evidence for physical and functional interactions between U19/Eaf2 and pVHL, a well-established tumor suppressor.

The *U19/Eaf2* knockout mice have diverse phenotypes in different tissues. We previously reported that U19/Eaf2 can function as a tumor suppressor as evidenced by the development of B-cell lymphoma, hepatocellular carcinoma, lung adenocarcinoma, and prostatic intraepithelial neoplasia in *U19/Eaf2* knockout mice (30). Here, we show that *U19/Eaf2* deletion also caused various nontumorigenic abnormalities, including aspermatogenesis and extramedullary hematopoiesis (Fig. 1). The diverse phenotypes observed in *U19/Eaf2* knockout mice indicate that U19/Eaf2 could influence multiple cellular activities in various tissues and that U19/Eaf2 function seems to be cell type specific. In testes, *U19/Eaf2* deletion significantly enhanced apoptosis but had no effect on proliferation. In contrast, *U19/Eaf2* deletion enhanced proliferation but did not affect cell death in other organs such as the spleen. It is also interesting that the penetrance of *U19/Eaf2*-null mutation to develop each of the different phenotypes is not 100%. For example, the penetrance for the aspermatogenesis phenotype by *U19/Eaf2* knockout is only ~26%.

U19/Eaf2 may regulate diverse cellular activities by binding to different partners. It was previously reported that U19/Eaf2 binds to ELL family proteins and thereby affects ELL transcription elongation activities. The report that Eaf1, the homologue of U19/Eaf2, is a component of the Cajal body, a nuclear suborganelle involved in the biogenesis of small nuclear ribonucleoproteins, suggests that U19/Eaf2 may also contribute to the formation of small nuclear ribonucleoproteins (37). Identification and characterization of additional U19/Eaf2 binding partners will provide further insights into the mechanisms by which U19/Eaf2 regulates various cellular processes.

Identification of pVHL as a new U19/Eaf2 binding partner implicates a role for U19/Eaf2 in pVHL signaling, providing a novel mechanism in U19/Eaf2 action. The interaction between U19/Eaf2 and pVHL seems to be physiologically relevant. The cycloheximide inhibition and pulse-chase experiments provide strong evidence that U19/Eaf2 can prolong the half-life of pVHL in cultured cells (Fig. 4). The observations that MEF cells, testes, and other tissues derived from *U19/Eaf2* knockout mouse had less pVHL relative to controls argue that U19/Eaf2 indeed stabilizes pVHL *in vivo* (Fig. 4). Furthermore, several pieces of evidence indicate that the interaction has functional consequences. For example, *U19/Eaf2*-null cells had higher HIF1α protein levels than wild-type controls, particularly under hypoxic conditions (Fig. 5). The prompt and complete degradation of HIF1α following release from hypoxia in wild-type MEF cells was retarded in the *U19/Eaf2* knockout MEF cells. In addition, *U19/Eaf2* deletion significantly enhanced HRE activation. These findings argue that U19/Eaf2 loss results in the elevation of the VHL/HIF/HRE axis, a pathway known to control angiogenesis (38). As expected, Matrigel plug angiogenesis assays showed significantly enhanced neovascularization in *U19/Eaf2* knockout mice in response to VEGF (Fig. 6), providing evidence that U19/Eaf2 can modulate the vascular system presumably by binding to pVHL. At the same time, pVHL may also modulate the function of U19/Eaf2 because studies here show that the protein level of U19/Eaf2 is enhanced in the presence of *VHL* gene expression.

Like U19/Eaf2, pVHL has more than one binding partner; thus, U19/Eaf2- and pVHL-dependent signaling pathways are likely to be different but overlapping. A recent study identified pVHL as a binding partner of the tumor suppressor p53. Binding of pVHL led to an increase in both stability and transcriptional activation of p53, suggesting that other tumor suppressors might serve as mediators for the tumor-suppressive function of pVHL (39). In testes, the phenotypes are similar between the *U19/Eaf2* knockout and *VHL* conditional knockout mice, suggesting significant functional overlaps between U19/Eaf2 and pVHL in this tissue. This also suggests that one possible mechanism for aspermatogenesis in *U19/Eaf2*

knockout mice may involve pVHL. The function of pVHL in the testis is likely compromised in the absence of U19/Eaf2, which may cause a decrease in microtubule stability (40) and, subsequently, defects in both mitosis and meiosis leading to aspermatogenesis (7). The functional overlap between the U19/Eaf2 and pVHL axes may be less extensive in other tissues, given that *U19/Eaf2* knockout and *VHL* knockout did not display similar phenotypes outside of the testes. Future studies will be required to elucidate the functional significance of the cross talk between U19/Eaf2 and pVHL in the context of other binding partners.

In summary, our novel findings strongly argue that U19/Eaf2 is a new regulator of the pVHL pathway and provide compelling evidence of cooperation between the two tumor suppressors, U19/Eaf2 and pVHL.

Acknowledgments

Grant support: NIH grants R37 DK51193, R01 CA120386, and P50 CA90386. J. Ai is a recipient of the Mellam Family Foundation Fellowship.

We thank M. Celeste Simon and Paul G. Corn for their advice; Peter J. Ratcliffe, William G. Kaelin, Paul G. Corn, Wafik S. El-Deiry, Frank Lee, Navdeep Chandel, Katherine Rundell, Ralph Buttyan, and Robert Matusik for kindly providing us with reagents; Moira Hitchens and Minh Nguyen for editing and critical reading of the manuscript; and the members of the Wang lab for extensive discussions.

References

1. Kaelin WG Jr. Molecular basis of the VHL hereditary cancer syndrome. Nat Rev Cancer 2002;2:673–82. [PubMed: 12209156]
2. Herman JG, Latif F, Weng Y, et al. Silencing of the VHL tumor-suppressor gene by DNA methylation in renal carcinoma. Proc Natl Acad Sci U S A 1994;91:9700–4. [PubMed: 7937876]
3. Linehan WM, Lerman MI, Zbar B. Identification of the von Hippel-Lindau (VHL) gene. Its role in renal cancer JAMA 1995;273:564–70.
4. Linehan WM, Vasselli J, Srinivasan R, et al. Genetic basis of cancer of the kidney: disease-specific approaches to therapy. Clin Cancer Res 2004;10:6282–9S.
5. Gnarra JR, Ward JM, Porter FD, et al. Defective placental vasculogenesis causes embryonic lethality in VHL-deficient mice. Proc Natl Acad Sci U S A 1997;94:9102–7. [PubMed: 9256442]
6. Haase VH, Glickman JN, Socolovsky M, et al. Vascular tumors in livers with targeted inactivation of the von Hippel-Lindau tumor suppressor. Proc Natl Acad Sci U S A 2001;98:1583–8. [PubMed: 11171994]
7. Ma W, Tessarollo L, Hong SB, et al. Hepatic vascular tumors, angiectasis in multiple organs, and impaired spermatogenesis in mice with conditional inactivation of the VHL gene. Cancer Res 2003;63:5320–8. [PubMed: 14500363]
8. Maxwell PH, Wiesener MS, Chang GW, et al. The tumour suppressor protein VHL targets hypoxia-inducible factors for oxygen-dependent proteolysis. Nature 1999;399:271–5. [PubMed: 10353251]
9. Ohh M, Park CW, Ivan M, et al. Ubiquitination of hypoxia-inducible factor requires direct binding to the β-domain of the von Hippel-Lindau protein. Nat Cell Biol 2000;2:423–7. [PubMed: 10878807]
10. Pause A, Lee S, Worrell RA, et al. The von Hippel-Lindau tumor-suppressor gene product forms a stable complex with human CUL-2, a member of the Cdc53 family of proteins. Proc Natl Acad Sci U S A 1997;94:2156–61. [PubMed: 9122164]
11. Lonergan KM, Iliopoulos O, Ohh M, et al. Regulation of hypoxia-inducible mRNAs by the von Hippel-Lindau tumor suppressor protein requires binding to complexes containing elongins B/C and Cul2. Mol Cell Biol 1998;18:732–41. [PubMed: 9447969]
12. Lisztwan J, Imbert G, Wirbelauer C, et al. The von Hippel-Lindau tumor suppressor protein is a component of an E3 ubiquitin-protein ligase activity. Genes Dev 1999;13:1822–33. [PubMed: 10421634]
13. Ohh M, Takagi Y, Aso T, et al. Synthetic peptides define critical contacts between elongin C, elongin B, and the von Hippel-Lindau protein. J Clin Invest 1999;104:1583–91. [PubMed: 10587522]

14. Stebbins CE, Kaelin WG Jr, Pavletich NP. Structure of the VHL-ElonginC-ElonginB complex: implications for VHL tumor suppressor function. Science 1999;284:455–61. [PubMed: 10205047]
15. Kamura T, Conrad MN, Yan Q, et al. The Rbx1 subunit of SCF and VHL E3 ubiquitin ligase activates Rub1 modification of cullins Cdc53 and Cul2. Genes Dev 1999;13:2928–33. [PubMed: 10579999]
16. Kamura T, Koepp DM, Conrad MN, et al. Rbx1, a component of the VHL tumor suppressor complex and SCF ubiquitin ligase. Science 1999;284:657–61. [PubMed: 10213691]
17. Bruick RK, McKnight SL. A conserved family of prolyl-4-hydroxylases that modify HIF. Science 2001;294:1337–40. [PubMed: 11598268]
18. Epstein AC, Gleadle JM, McNeill LA, et al. Elegans EGL-9 and mammalian homologs define a family of dioxygenases that regulate HIF by prolyl hydroxylation. Cell 2001;107:43–54. [PubMed: 11595184]
19. Jaakkola P, Mole DR, Tian YM, et al. Targeting of HIF-α to the von Hippel-Lindau ubiquitylation complex by O_2-regulated prolyl hydroxylation. Science 2001;292:468–72. [PubMed: 11292861]
20. Ivan M, Kondo K, Yang H, et al. HIFα targeted for VHL-mediated destruction by proline hydroxylation: implications for O_2 sensing. Science 2001;292:464–8. [PubMed: 11292862]
21. Hon WC, Wilson MI, Harlos K, et al. Structural basis for the recognition of hydroxyproline in HIF-1α by pVHL. Nature 2002;417:975–8. [PubMed: 12050673]
22. Min JH, Yang H, Ivan M, et al. Structure of an HIF-1α-pVHL complex: hydroxyproline recognition in signaling. Science 2002;296:1886–9. [PubMed: 12004076]
23. Semenza GL. HIF-1 and human disease: one highly involved factor. Genes Dev 2000;14:1983–91. [PubMed: 10950862]
24. de Paulsen N, Brychzy A, Fournier MC, et al. Role of transforming growth factor-α in von Hippel-Lindau (VHL)(−/−) clear cell renal carcinoma cell proliferation: a possible mechanism coupling VHL tumor suppressor inactivation and tumorigenesis. Proc Natl Acad Sci U S A 2001;98:1387–92. [PubMed: 11171960]
25. Kourembanas S, Hannan RL, Faller DV. Oxygen tension regulates the expression of the platelet-derived growth factor-B chain gene in human endothelial cells. J Clin Invest 1990;86:670–4. [PubMed: 2384608]
26. Semenza GL. Regulation of mammalian O_2 homeostasis by hypoxia-inducible factor 1. Annu Rev Cell Dev Biol 1999;15:551–78. [PubMed: 10611972]
27. Maranchie JK, Vasselli JR, Riss J, et al. The contribution of VHL substrate binding and HIF1-α to the phenotype of VHL loss in renal cell carcinoma. Cancer Cell 2002;1:247–55. [PubMed: 12086861]
28. Carmeliet P, Dor Y, Herbert JM, et al. Role of HIF-1α in hypoxia-mediated apoptosis, cell proliferation and tumour angiogenesis. Nature 1998;394:485–90. [PubMed: 9697772]
29. Acker T, Diez-Juan A, Aragones J, et al. Genetic evidence for a tumor suppressor role of HIF-2α. Cancer Cell 2005;8:131–41. [PubMed: 16098466]
30. Xiao W, Zhang Q, Habermacher G, et al. U19/Eaf2 knockout causes lung adenocarcinoma, B-cell lymphoma, hepatocellular carcinoma and prostatic intraepithelial neoplasia. Oncogene 2008;27:1536–44. [PubMed: 17873910]
31. Herbst A, Tansey WP. HAM: a new epitope-tag for *in vivo* protein labeling. Mol Biol Rep 2000;27:203–8. [PubMed: 11455955]
32. Zhu N, Wang Z. Calreticulin expression is associated with androgen regulation of the sensitivity to calcium ionophore-induced apoptosis in LNCaP prostate cancer cells. Cancer Res 1999;59:1896–902. [PubMed: 10213498]
33. Xiao W, Zhang Q, Jiang F, et al. Suppression of prostate tumor growth by U19, a novel testosterone-regulated apoptosis inducer. Cancer Res 2003;63:4698–704. [PubMed: 12907652]
34. Emerling BM, Platanias LC, Black E, et al. Mitochondrial reactive oxygen species activation of p38 mitogen-activated protein kinase is required for hypoxia signaling. Mol Cell Biol 2005;25:4853–62. [PubMed: 15923604]
35. Akhtar N, Dickerson EB, Auerbach R. The sponge/Matrigel angiogenesis assay. Angiogenesis 2002;5:75–80. [PubMed: 12549862]
36. Wilasrusmee C, Yusupov I, Ondocin P, et al. Angiocidal effect of cyclosporin A: a new therapeutic approach for pathogenic angiogenesis. Int Angiol 2005;24:372–9. [PubMed: 16355096]

37. Polak PE, Simone F, Kaberlein JJ, et al. ELL and EAF1 are Cajal body components that are disrupted in MLL-ELL leukemia. Mol Biol Cell 2003;14:1517–28. [PubMed: 12686606]

38. Kaelin WG. The von Hippel-Lindau tumor suppressor protein: roles in cancer and oxygen sensing. Cold Spring Harb Symp Quant Biol 2005;70:159–66. [PubMed: 16869749]

39. Roe JS, Kim H, Lee SM, Kim ST, Cho EJ, Youn HD. p53 stabilization and transactivation by a von Hippel-Lindau protein. Mol Cell 2006;22:395–405. [PubMed: 16678111]

40. Hergovich A, Lisztwan J, Barry R, et al. Regulation of microtubule stability by the von Hippel-Lindau tumour suppressor protein pVHL. Nat Cell Biol 2003;5:64–70. [PubMed: 12510195]

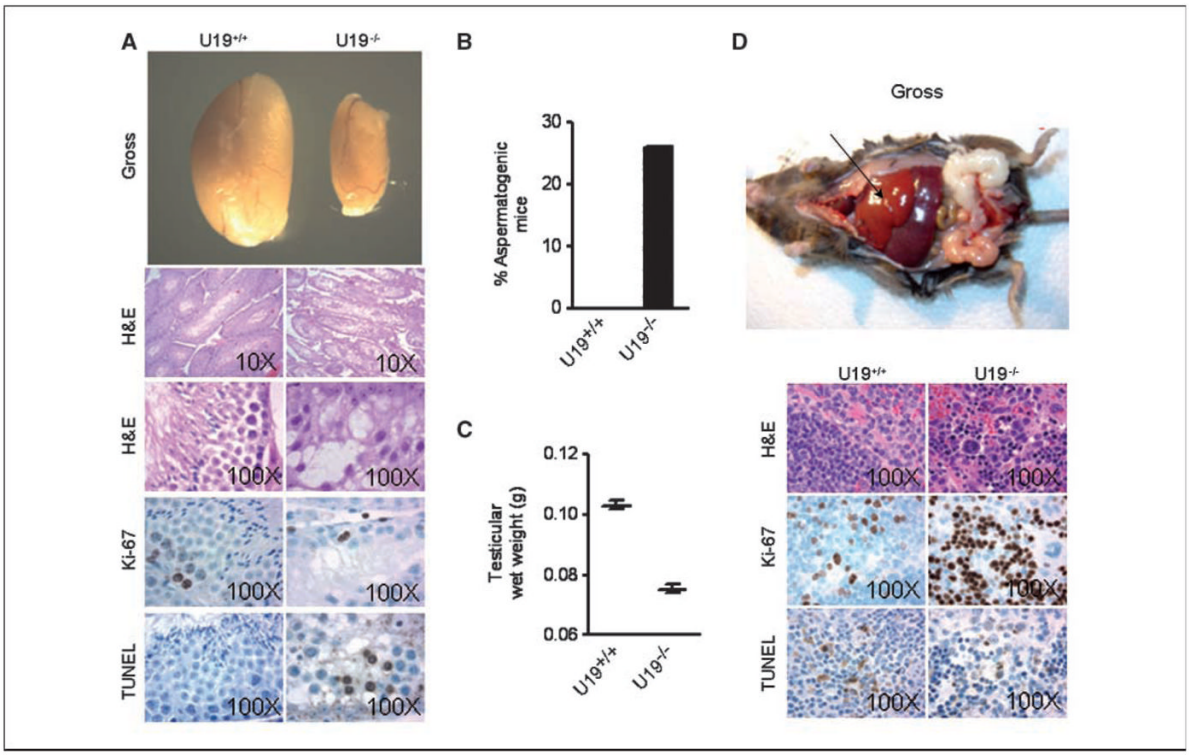

Figure 1.

Nonmalignant phenotypes in *U19/Eaf2*-null mice ages ≥22 mo. *A*, a representative wild-type testis and a regressed $U19^{-/-}$ testis in old mice. The pictures show gross, H&E (10× and 100× objectives), Ki-67 (100× objective), and TUNEL (100× objective) stainings of the wild-type testis and the regressed *U19/Eaf2*-null testis. *B*, incidence rate of aspermatogenesis in wild-type and $U19^{-/-}$ mice. *C*, wet weight of testis in wild-type ($U19^{+/+}$) and *U19/Eaf2*-null ($U19^{-/-}$) mice. *D*, extramedullary hemopoiesis in $U19^{-/-}$ mice. *Top*, an animal with extramedullary hemopoiesis (*arrow*). *Bottom*, H&E, Ki-67, and TUNEL stainings (100× objective) of the wild-type and *U19/Eaf2*-null spleen.

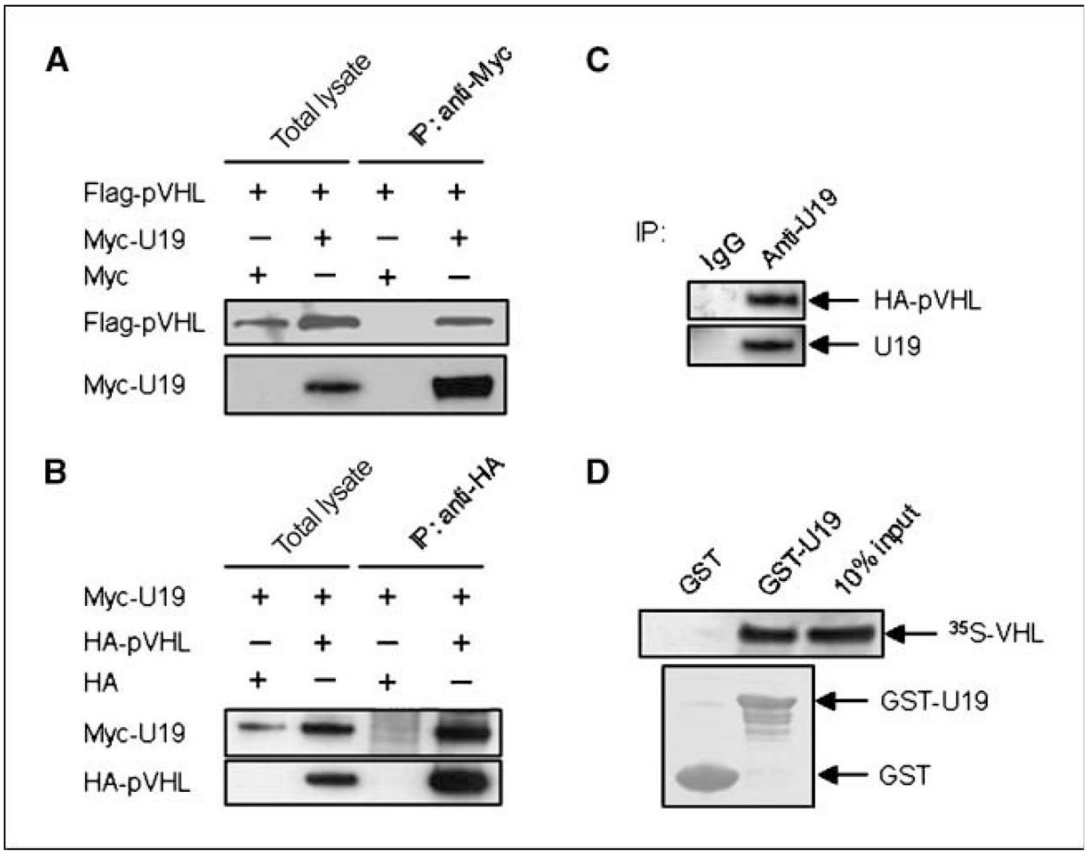

Figure 2.

Interaction of U19/Eaf2 with pVHL. *A*, Flag-tagged pVHL was cotransfected with Myc-tagged U19/Eaf2 or empty Myc vector into Cos-7 cells. Cell lysates were immunoprecipitated (*IP*) with anti-Myc antibody–conjugated agarose beads, and blots were probed with anti-Flag antibody (*top image*) or anti-Myc antibody (*bottom image*). *B*, Myc-U19 was cotransfected with HA-pVHL or empty HA vector into 293 cells. Cell lysates were immunoprecipitated with anti-HA antibody–conjugated agarose beads, and blots were probed with anti-Myc antibody (*top image*) or anti-HA antibody (*bottom image*). *C*, whole-cell lysates from RCC4/VHL cells exposed to hypoxia (1% O_2) for 16 h were subjected to immunoprecipitation with control rabbit IgG or rabbit anti-U19/Eaf2 polyclonal antibody, separated by SDS-PAGE, and immunoblotted with anti-HA and anti-U19/Eaf2 antibodies. *D*, *in vitro* translated ^{35}S-labeled pVHL was incubated with bacterially purified GST-U19/Eaf2 fusion protein attached to glutathione-agarose beads. GST served as negative control. After incubation, the beads were extensively washed and subjected to SDS-PAGE. Association of ^{35}S-VHL and U19/Eaf2 *in vitro* was detected by autoradiography. *Bottom image*, inputs of GST and GST fusion proteins are shown as Coomassie blue–stained gel.

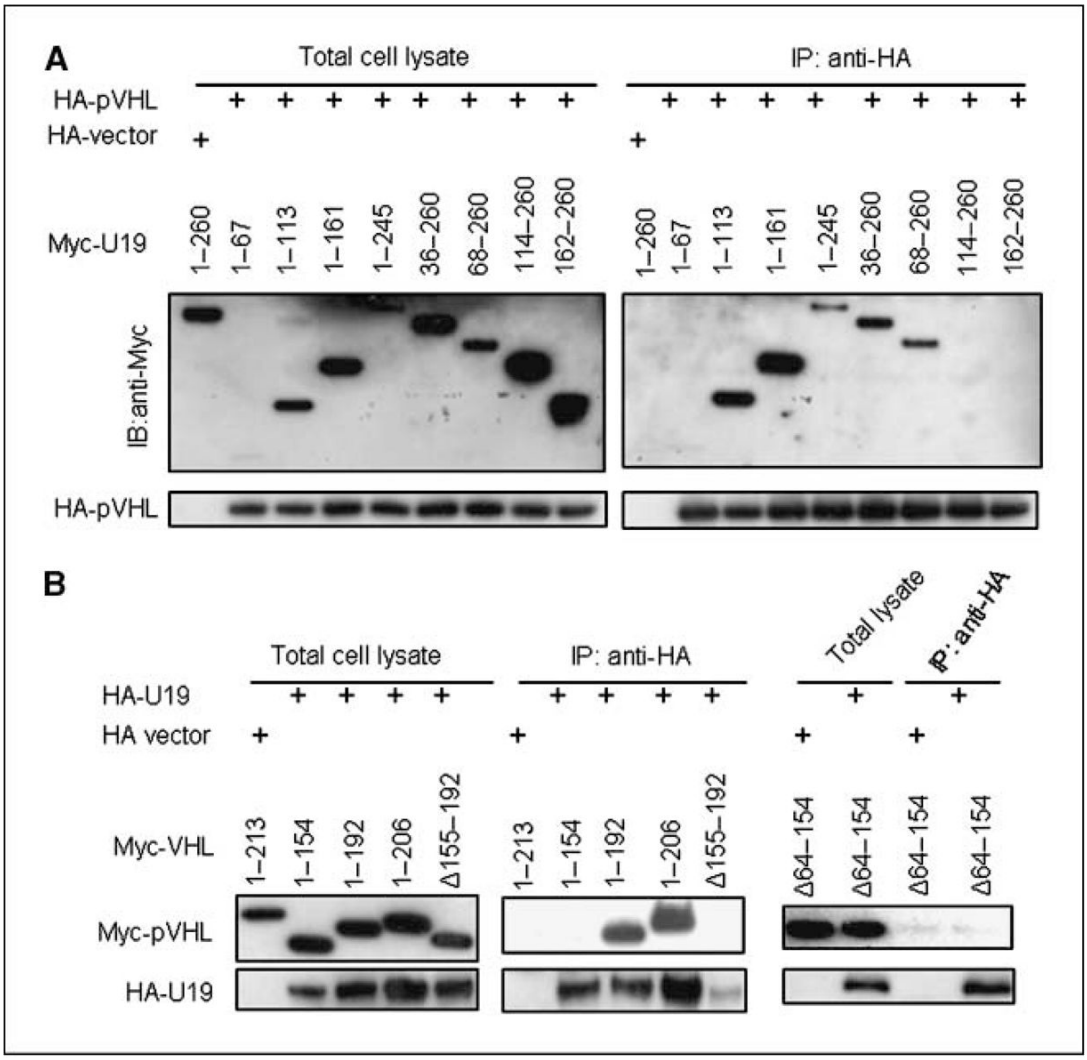

Figure 3.

Domain mapping of the interaction between U19/Eaf2 and pVHL. *A*, pVHL interacted with the NH_2-terminal region of U19/Eaf2 in coimmunoprecipitation assays. HA-pVHL was cotransfected with Myc-tagged U19/Eaf2 COOH-terminal deletion mutants (1–67, 1–113, 1–161, and 1–245) and NH_2-terminal deletion mutants (36–260, 68–260, 114–260, and 162–260) into 293 cells. Wild-type Myc-U19/Eaf2 was cotransfected with HA empty vector as a negative control. Cell lysates were immunoprecipitated with anti-HA antibody–conjugated agarose beads, and blots were probed with anti-Myc antibody (*top image*) or anti-HA antibody (*bottom image*). *B*, both the α and β domains of pVHL were required for interaction with U19/Eaf2 in coimmunoprecipitation assays. HA-U19/Eaf2 was cotransfected with the Myc-tagged major β domain (1–154), α and major β domains (1–192), α and entire β domains, α domain deletion mutant (Δ155–192), or major β domain deletion mutant (Δ64–154) into 293 cells. Wild-type Myc-pVHL cotransfected with HA empty vector served as a negative control. Cell lysates were immunoprecipitated with anti-HA antibody–conjugated agarose beads, and blots were probed with anti-Myc antibody (*top image*) or anti-HA antibody (*bottom image*).

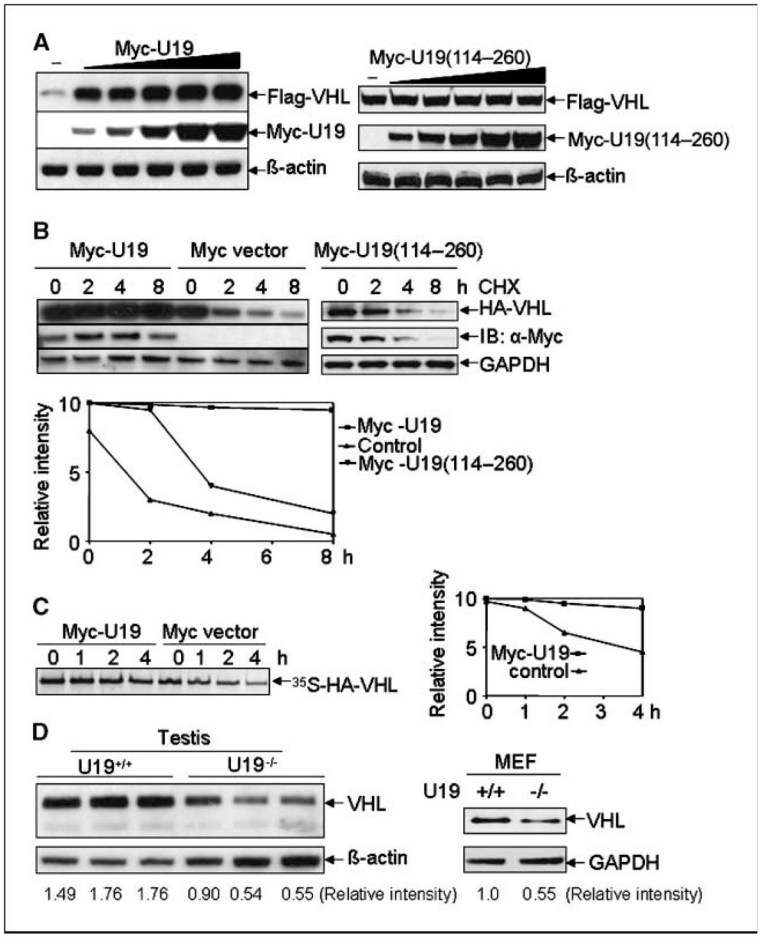

Figure 4.

Stabilization of pVHL by U19/Eaf2. *A*, the effect of wild-type U19/Eaf2 (*left*) or U19/Eaf2 deletion mutant (114–260; *right*) expression on transfected pVHL protein levels. *Left*, Cos-7 cells were cotransfected with 2.0 μg of Flag-VHL in the absence (−) or presence of increasing amounts of Myc-U19. Myc empty vector was used to complement the Myc-U19. *Right*, 293 cells were cotransfected with 2.0 μg of Flag-VHL in the absence (−) or presence of increasing amounts of Myc-U19 (114–260). Myc empty vector was used to complement the Myc-U19 (114–260). *B*, effect of U19/Eaf2 on pVHL protein stability. Two micrograms of HA-VHL were cotransfected with 2.0 μg of Myc-U19/Eaf2, Myc empty vector, or Myc-U19/Eaf2 (114–260) into 293 cells. Twenty hours after transfection, cells were treated with cycloheximide (*CHX*) at 50 μg/mL for the indicated number of hours. *C*, pulse-chase assay to determine HA-VHL protein half-life in the absence or presence of Myc-U19/Eaf2. Two micrograms of HA-VHL expression vector were cotransfected with Myc-U19/Eaf2 or Myc vector into 293 cells. Forty-eight hours after transfection, cells were metabolically labeled with [^{35}S]Met/Cys for 2 h followed by pulse-chase analysis for the indicated time periods. HA-VHL was immunoprecipitated from the cell lysate with anti-HA antibody–conjugated agarose beads and signals were detected by autoradiography. *D*, endogenous pVHL expression in the testes and MEF cells derived from U19$^{+/+}$ and U19$^{-/-}$ mice. Testes from three wild-type and three *U19/Eaf2* knockout mice were used. Two of the three *U19/Eaf2* knockout testes were normally sized, whereas the third (*center*) was reduced. The lack of U19/Eaf2 expression in the *U19/Eaf2*-null MEFs was verified (30). Blots of the testicular tissue were probed with anti-pVHL, anti–β-actin, or anti–glyceraldehyde-3-phosphate dehydrogenase (*GAPDH*) antibodies. The

relative expression level of pVHL was quantitated using the Photoshop CS 7.0 software and normalized to β-actin or GAPDH expression.

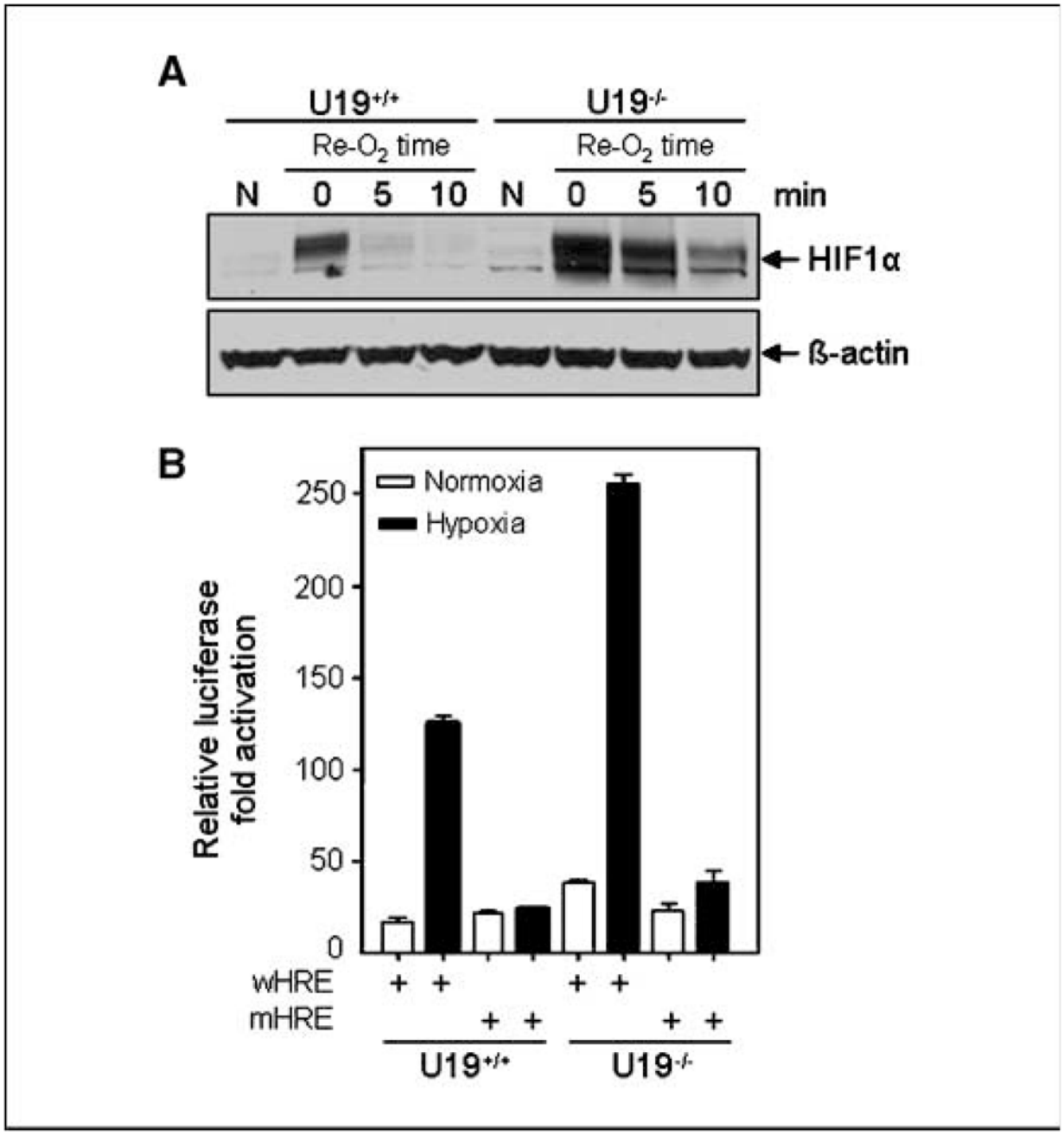

Figure 5.

U19/Eaf2 modulation of the protein level and transcriptional activity of HIF1α. *A*, the degradation kinetics of HIF1α in wild-type and $U19^{-/-}$ MEFs following release from hypoxia. $U19^{+/+}$ and $U19^{-/-}$ MEFs were maintained in a hypoxia chamber (~1% O_2) for 16 h to achieve HIF1α stabilization and then released into normoxia. The lysates were collected at the indicated time points for Western blot analysis of HIF1α. *B*, HIF1α transcriptional activity in wild-type and *U19/Eaf2*-null MEF cells. MEF cells were transiently transfected with wild-type (*wHRE*) or mutant (*mHRE*) reporter constructs, and transcriptional activity was measured after 16 h in normoxic (21% O_2) or hypoxic (1% O_2) conditions.

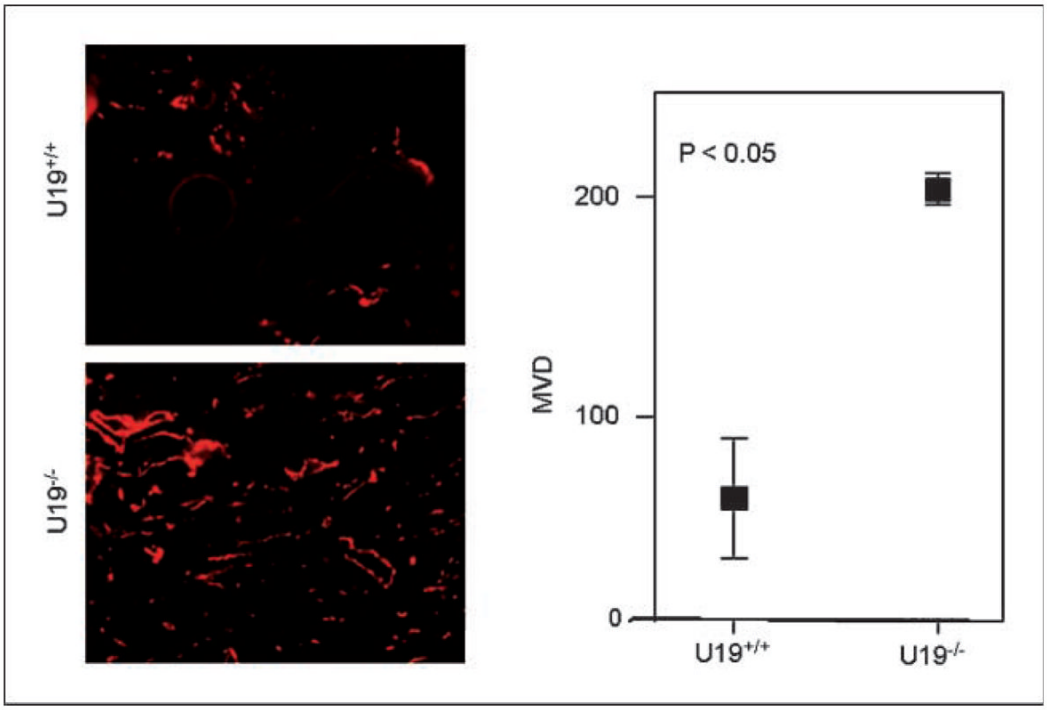

Figure 6.
The effect of *U19/Eaf2* deletion on angiogenesis in Matrigel plugs s.c. implanted in mice. *Left*, representative digital images of microvessels, stained with anti-CD31 antibody, in Matrigel plugs in the presence of 2 ng/mL VEGF in the wild-type and *U19/Eaf2* knockout mice. *Right*, quantitative analysis of the microvessel densities (*MVD*) in the Matrigel plugs.